Protein Medium Facilitates Electron Transfer in Photosynthetic Heliobacterial Reaction Center

Article *in* The Journal of Physical Chemistry B · September 2024

DOI: 10.1021/acs.jpcb.4c04956

4 authors:

Adam Pirnia
Arizona State University
2 PUBLICATIONS **2** CITATIONS
SEE PROFILE

Setare M Sarhangi
Iran University of Science and Technology
18 PUBLICATIONS **90** CITATIONS
SEE PROFILE

Abhishek Singharoy
University of Illinois, Urbana-Champaign
135 PUBLICATIONS **4,280** CITATIONS
SEE PROFILE

Dmitry Matyushov
Arizona State University
254 PUBLICATIONS **4,602** CITATIONS
SEE PROFILE

Protein Medium Facilitates Electron Transfer in Photosynthetic Heliobacter Reaction Center

Journal:	*The Journal of Physical Chemistry*
Manuscript ID	jp-2024-049565.R1
Manuscript Type:	Article
Date Submitted by the Author:	n/a
Complete List of Authors:	Pirnia, Mohammad Mehdi; Arizona State University, School of Molecular Sciences Mostajabi Sarhangi, Setare; Arizona State University, School of Molecular Sciences and Department of Physics Singharoy, Abhishek; Arizona State University, School of Molecular Sciences, Biodesign Center for Applied Structural Discovery Matyushov, Dmitry; Arizona State University, School of Molecular Sciences

Protein Medium Facilitates Electron Transfer in Photosynthetic Heliobacter Reaction Center

Mohammad Mehdi Pirnia,[†] Setare Mostajabi Sarhangi,[‡] Abhishek Singharoy,[†] and Dmitry V. Matyushov*,[¶]

†*School of Molecular Sciences, Arizona State University, PO Box 871504, Tempe, AZ 85287-1504, USA*

‡*Department of Physics, Arizona State University, PO Box 871504, Tempe, AZ 85287-1504, USA*

¶*School of Molecular Sciences and Department of Physics, Arizona State University, PO Box 871504, Tempe, AZ 85287-1504, USA*

E-mail: dmitrym@asu.edu

Abstract

This computational study addresses the question of how large membrane-bound proteins of electron transport chains facilitate fast vectorial charge transport. We study electron transfer reactions following ultrafast initial charge separation induced by absorption of light by P_{800} primary pair and leading to the electron localization at the A_0 cofactor. Two subsequent, much slower, reactions, electron transfer to the iron-sulfur cluster F_x and reduction of the menaquinone (MQ) cofactor, are studied by combining molecular dynamics simulations, electronic structure calculations, and theoretical modeling. The low value of the electronic coupling between A_0 and F_x brings this reaction to the microsecond time scale even at zero activation barrier. In contrast, A_0-MQ electron transfer occurs on a sub-nanosecond time scale and might become the preferred route for charge transport. We elucidate mechanistic properties of the protein medium allowing fast, vectorial charge transfer. The electric field is high and inhomogeneous inside the protein and is coupled to high polarizabilities of cofactors to significantly lower the reaction barrier. The A_0-MQ separation puts this reaction at the edge between the plateau characterizing reaction dynamical control and exponential falloff due to electronic tunneling. A strong separation in relaxation times of the medium dynamics for the forward and backward reactions promotes vectorial charge transfer.

TOC Graphic

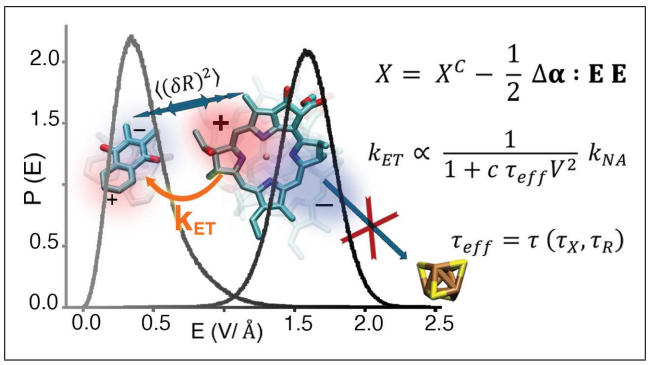

Introduction

Enzymes catalyze chemical reaction and, according to the widely accepted Pauling's paradigm,[1] catalytic action is related to lowering (stabilization) of the transition-state free energy compared to a reference reaction. A recent support of this idea has arrived from measurements of electric fields in active sites of enzymes. An inhomogeneous distribution of charge in a folded protein creates an electric field of $\simeq 1.4$ V/Å sufficient to stabilize the transition state with a dipolar character.[2,3] Despite significant supporting evidence, Pauling's idea clashes with another highly successful theory of chemical reactivity when applied to protein electron transfer. The Marcus theory[4] stipulates that only equilibrium properties, which are the first and second statistical moments of the energy-gap reaction coordinate[5] at two charge-transfer equilibrium configurations are required to determine the activation barrier. No calculations or measurements of the solvation free energy in the transition-state configuration enter the theory which specifies the barrier from equilibrium configurations that can be quite distinct from the transition state. This fundamental difference in approaching the free energy of activation is of general significance for the understanding of mechanisms and efficiency of biological energy chains,[6] but also presents a conceptual challenge to the quest to interrogate physical foundations of enzyme catalysis.[7] The general issues involved are whether the equilibrium statistics is always adequate[8] and whether dynamical identities of proteins affect enzymatic reaction rates.[9–11] These issues are related since the position of the reaction rate within the frequency spectrum of the protein-water fluctuations specifies the non-equilibrium free energy of activation which is distinct from the corresponding Gibbs energy.[8]

Proteins are clearly capable of significantly lowering the activation energy for electron transfer through the reduction of the Marcus reorganization energy of electron transfer relative to reference reactions in solution.[12] The reorganization energy thus becomes a key parameter for biological electron transport given that reaction driving forces are often low for individual electron hops in biological electron transport chains.[6] Another significant parameter is the electronic coupling[13] V entering the pre-exponential factor of the nonadiabatic

electron-transfer rate constant,[14–16] $k_{\mathrm{NA}} \propto V^2$.

Early attempts to fit Marcus theory to rates measured in bacterial photosynthesis resulted in a "universal" reorganization energy of $\simeq 0.8$ eV for protein electron transfer,[17] leaving V and the reaction Gibbs energy ΔG as the only parameters to tune and optimize biological charge transport. With the growing sophistication of protein computer simulations, an increasing number of recent studies have reported reorganization energies for protein electron transfer.[18–20] These calculations, based on the statistics of Coulomb interactions between the transferred electron and the protein/water medium,[4,21] often produce numbers much higher than the values derived from measured reaction kinetics, reaching the magnitudes of $1.0 - 2.0$ eV for different systems.[22] It was suggested that the discrepancy lies in the neglect of screening of Coulomb interaction by induced electronic polarization in standard simulation protocols employing non-polarizable force fields.[23] However, modeling of electronic polarization effects[22,24] requires a reduction of the reorganization energy from nonpolarizable force fields only by a factor of $\simeq 0.8$. This correction cannot account for the differences between empirical and calculated reaction barriers. Moreover, protein thin-film electrochemistry[25–27] and electrochemical atomic force microscopy[28,29] have consistently reported reorganization energies far below the anticipated "universal" value, in the range of $0.1 - 0.5$ eV. To summarize, the standard framework of evaluating the reorganization energy from the statistic of electrostatic interactions[21] consistently yields activation barriers which are too high to explain observations. Apart from technical challenges of developing better calibrated force fields, this discrepancy calls for an inquiry into fundamental mechanisms for lowering barriers for electron hops in the protein thermal bath. One wonders if nature has prepared more tricks than one would anticipate solely from the statistics of electrostatic interactions. This study is a step to address these challenges.

The inquiry of what is special about proteins as conduits for charge transport is far from resolved. Clearly, natural photosynthesis relies on fast charge separation following photoexcitation to avoid wasteful recombination pathways.[30,31] The challenge to understand

physical mechanisms behind catalysis and overall efficiency of charge transport is not limited to natural energy chains, but extends to a recently posed puzzle on an unusually high conductivity of proteins lacking redox cofactors[32–34] and high conductivity of cytochrome nanowires enabling extracellular electron transport in anaerobic bacterial respiration.[35,36]

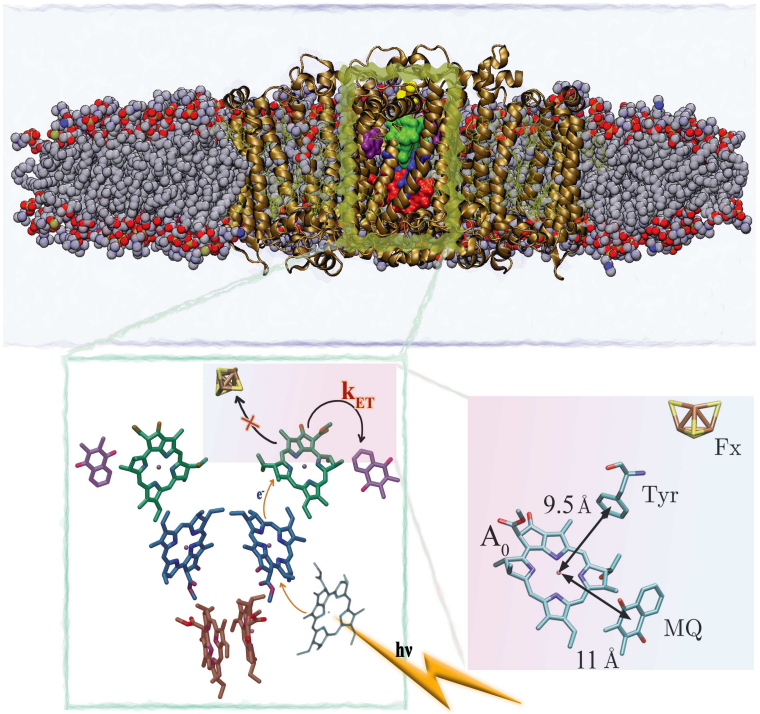

Figure 1: Electron transfer cofactors of the *H. modesticaldum* reaction center (HbRC). The upper panel shows the MD simulation setup. The lower left panel shows the pathway of electron transport in the HbRC following photoexcitation. The right lower panel zooms in to cofactors considered in this paper, also showing the distances between A_0 and menaquinone (MQ) cofactors for the forward electronic transition. The Tyr residue potentially participating in superexchange coupling to the iron-sulfur cluster (F_x) is also shown.

This paper presents high-performance molecular dynamic (MD) simulations, theoretical quantum calculations, and formal modeling of two electron-transfer steps in bacterial *H. modesticaldum* reaction center (HbRC) the X-ray structure of which has recently became available.[37] HbRC contains an iron-sulfur cluster, characteristic of Type I reaction centers (RCs) also common to Photosystem I in cyanobacteria and plants.[37] Heliobacteria share a common ancestor with cyanobacteria and Chlorobi (green sulfur bacteria), and their RCs are viewed as earliest evolved.[38] Given these factors, and due to its relatively simple structure

compared to other organisms, HbRC offers valuable insights into the evolution of natural photosynthesis.

The simulation model is complex (Figure 1), including 275,000 atoms, of which about 20,000 belong to the protein made of 1,252 residues (Supporting Information, SI). There are additionally $\simeq$ 70 cofactors in the protein core, including 38 Bchl-g, -g' and two 8(1)-OH-chlorophylls a_F, and one iron-sulfur cluster F_x.[37] Two menaquinones (MQ) were manually added to the system, replacing analogs that were potentially present there during the purification process. The MD simulations are classical, in contrast to many existing algorithms of polarizable embedding.[39–41] The polarizabilities of the cofactors are added at the analysis stage, through the gas-phase polarizabilities of the cofactors calculated separately (SI) and the electric field of the medium calculated from classical MD trajectories (see below).

This study asks the following question: What are the generic properties of the protein-water-membrane thermal bath promoting efficient vectorial charge transport? We start our analysis with outlining key concepts of protein charge transfer that are implemented in specific calculations. The focus here is on physical mechanisms rather than on technical aspects presented in the SI.

Results

Physical Concepts. Calculations for two electron-transfer reactions are presented in this study. The cofactor A_0 (Figure 1) is viewed as the electron donor (D) delivering the electron to two acceptor (A) cofactors: F_x and MQ. The initial states (1) for these two reactions are $A_0^- - F_x$ and $A_0^- - MQ$. The final states (2) are $A_0 - F_x^-$ and $A_0 - MQ^-$. Two reactions and four electron-transfer states are considered and modeled by the molecular dynamics (MD) simulations

$$\begin{array}{ll} (1) & A_0^- + F_x \longrightarrow A_0 + F_x^- \quad (2), \\ (1) & A_0^- + MQ \longrightarrow A_0 + MQ^- \quad (2) \end{array} \tag{1}$$

For both reactions, two charge-transfer states are specified by the index $i = 1, 2$ as shown in the reaction scheme.

Given high intensity of internal electric fields, $\simeq$ 1.4 V/Å, inside proteins,[2,3] our first question is how can it contribute to lowering the activation barriers for electronic hops. Such a mechanism is indeed offered by combining strong electric fields with high electronic polarizability of electron-transfer cofactors.[42–44] Our MD simulations show that the electric field magnitude at one of the cofactors, A_0, is comparable to those found in active sites of enzymes[2,3] (Figure 2a). Below we present quantum calculations of cofactors polarizabilities, which are combined with the statistics of the electric field from MD to estimate the effect of the protein electric field on the activation barrier. Many cofactors present in biological energy chains (porphyrins, hemes, bacteriochlorophylls, etc[30]) are highly polarizable conjugate molecules. It is still not entirely clear whether high polarizability, coupled to strong protein electric fields,[45] is essential for the charge-transfer function, but we arrive to an affirmative answer in the case of electron transfer between A_0 and MQ cofactors (Figure 1).

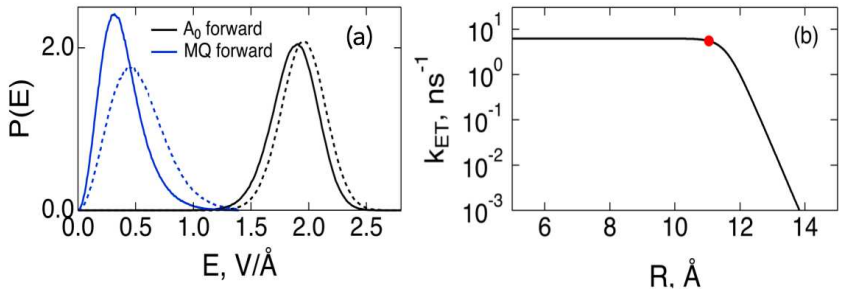

Figure 2: (a) Normalized distributions of the electric-field magnitude at A_0 and MQ cofactors of the RC. The solid lines indicate forward transition and the dashed lines refer to backward transitions. (b) Rate constant between A_0 and MQ cofactors vs the distance R between them calculated with the parameters from MD simulations and quantum calculations. The red point indicates the rate at the average distance between A_0 and MQ for the forward transition.

The appearance of molecular polarizability in the description of electron transfer alters the basic Marcus phenomenology of reaction activation[4] operating in terms of a single reorganization energy λ and the reaction free energy (negative of the driving force) ΔG. This

description is sufficient for the picture of shifted crossing parabolas. In contrast, polarizable systems make free energy surfaces of electron transfer non-parabolic,[42] thus requiring more than one reorganization energy.

Polarizable systems are formally described by the Q-model of electron transfer,[42,46] which is based on three parameters, in contrast to two parameters (λ and ΔG) in Marcus theory. The Q-model recognizes that a single reorganization energy of Marcus theory has to be replaced with three different reorganization energies. The first one comes from the separation of two minima of the electron-transfer free energy surfaces. Being closely related to the Stokes shift in spectroscopy, it carries the name of the Stokes-shift reorganization energy λ^{St}. It is specified by the difference between average values $\langle X\rangle_i$ of the energy gap X (defined below) between states 1 and 2

$$\lambda^{\mathrm{St}} = \frac{1}{2}\left(\langle X\rangle_1 - \langle X\rangle_2\right) \tag{2}$$

Two other reorganization energies λ_i are specified by variances of the energy gap in two charge-transfer states

$$\lambda_i = \frac{1}{2k_{\mathrm{B}}T}\langle(\delta X)^2\rangle_i, \quad \delta X = X - \langle X\rangle_i \tag{3}$$

One arrives at free-energy surfaces of electron transfer in terms of three distinct reorganization energies. Crossing of these surfaces at the tunneling configuration, $X = 0$, specifies the activation barrier. The Q-model[46] requires λ^{St} to fall between two λ_i and needs only two out of three reorganization energies for full modeling. Charge transfer in proteins involves more potential sources of nonlinearity than just polarizability of the cofactors and we do not expect full mapping of simulations on the Q-model. However, the general phenomenology of non-parabolic free energy surfaces with non-equal reorganization energies is confirmed by our analysis.

Another essential parameter specified by the architecture of biological energy chains is the distance R between the cofactors. It limits the length of electronic tunneling through electronic coupling $V_i(R)$, $i = 1, 2$, which decays exponentially[13] with R as specified by the

distance decay parameter γ

$$V_i(R) = V_{e,i} e^{-\frac{1}{2}\gamma \delta R}, \quad \delta R = R - R_{e,i} \tag{4}$$

Here, $R_{e,i} = \langle R \rangle_i$ is the equilibrium donor-acceptor distance and $V_{e,i} = V(R_{e,i})$ is the equilibrium coupling. The exponential falloff of the tunneling probability limits the distance between the cofactors to the Dutton radius[47] $R_D \simeq 14$ Å for activated transition and to $\simeq 21$ Å for activationless electron transfer.[48]

The standard Golden-rule (non-adiabatic, NA) reaction rate is proportional to electronic coupling V_i squared,[14] $k_{\mathrm{NA},i} \propto V_i^2$. However, the tunneling rate competes with the rate of energy dissipation at the top of the activation barrier,[49–52] modifying the rate constant pre-exponential factor in the region of dynamical control of electron transfer, when the rate constant becomes proportional to the inverse medium relaxation time. When the picture of dynamical medium control is extended to reactions in proteins, one has to consider at least two medium modes with competing dynamics: Stokes-shift dynamics (dynamics of electrostatic interactions[53]) and the dynamics of the donor-acceptor distance.[15,54,55] To obtain the rate constant of electron transfer k_{ET}, the nonadiabatic rate constant k_{NA} is modified with the dynamical correction factor $1 + g$

$$k_{\mathrm{ET}} = (1+g)^{-1} k_{\mathrm{NA}} \propto \frac{V^2}{1+g} e^{-\beta \Delta F^\dagger} \tag{5}$$

where $\beta = (k_{\mathrm{B}} T)^{-1}$ is the inverse temperature and $\Delta F^\dagger$ is the activation free energy of electron transfer; the subscript "i" specifying the state has been dropped for brevity. The crossover parameter

$$g \propto V^2 \tau_{\mathrm{eff}} \tag{6}$$

is proportional to the product of V^2 and the effective medium relaxation time τ_{eff} affected by the Stokes-shift and distance dynamics. When $g > 1$, either because of a large electronic

coupling or because of slow relaxation, V^2 cancel out in the nominator and denominator in eq 5. The reaction dynamics enters the regime of Kramers kinetics,[56,57] $k_{\rm ET} \propto \tau_{\rm eff}^{-1}$, when the rate is unaffected by electronic tunneling and becomes independent of the donor-acceptor distance. The crossover distance R^*, determined by the condition $g(R^*) = 1$, turns out[55] to be close to the empirically determined Dutton radius[47] $R_D \simeq 14$ Å. If this estimate is correct, most intraprotein electron-transfer reactions should fall either in the crossover region between dynamical control and tunneling or entirely in the regime of dynamical medium control.

We find below that the rate of electron transfer between A_0 and MQ is indeed controlled by the medium dynamics. The average distance between them (11.0 Å center-to-center) puts the reaction rate right at the "edge of the cliff" (red dot in Figure 2b): this is the largest distance that does not sacrifice the reaction rate. We now turn to the specifics of calculations leading to the rate constant shown in Figure 2b.

Free energy surfaces of electron transfer. The free energy surfaces of electron transfer are potentials of mean force along the reaction coordinate X equal to the energy separation between the final state when the electron is on the acceptor and the initial state with the electron on the donor.[19,21,42] The probability densities $P_i(X)$ produce two free energy surfaces for the forward, $i = 1$, and backward, $i = 2$, transitions

$$F_i(X) = F_{0i} - k_{\rm B}T \ln P_i(X) \tag{7}$$

where F_{0i} are equilibrium free energies in two electron-transfer states. Since F_{0i} are not provided by simulations, the functions $-k_{\rm B}T \ln P_i(X)$ in eq 7 are vertically shifted to reproduce the experimental reaction Gibbs energy $\Delta G_0 = F_{02} - F_{01}$ supplied by experiment. The free-energy surfaces are also shifted horizontally to cross at the tunneling configuration $X = 0$. This horizontal shift accommodates an unknown non-polar energy gap $\Delta E^{\rm np}$ entering X

$$X = \Delta E^{\rm np} + X^C - \frac{1}{2}\Delta\boldsymbol{\alpha}^D : \mathbf{E}^D\mathbf{E}^D - \frac{1}{2}\Delta\boldsymbol{\alpha}^A : \mathbf{E}^A\mathbf{E}^A \tag{8}$$

Here, X^C is the standard Coulomb component of the energy gap typically sampled in simulations of protein electron transfer[18,19,58]

$$X^C = \sum_j \Delta q_j^D \phi_j^D + \sum_j \Delta q_j^A \phi_j^A \tag{9}$$

The difference charges $\Delta q_j^D = q_j^{D,2} - q_j^{D,1}$ and $\Delta q_j^A = q_j^{A,2} - q_j^{A,1}$ provide changes of the atomic partial charges at the donor and acceptor in electronic transition. They interact with site electrostatic potentials ϕ_j^a; $a = \mathrm{D}, \mathrm{A}$. The second-rank tensors of polarizability difference between two oxidation states in eq 8, $\Delta\boldsymbol{\alpha}^D = \boldsymbol{\alpha}_2^D - \boldsymbol{\alpha}_1^D$ and $\Delta\boldsymbol{\alpha}^A = \boldsymbol{\alpha}_2^A - \boldsymbol{\alpha}_1^A$, have to be considered separately since they depend on orientations of cofactors in the protein matrix (see SI). They are contracted with electrostatic fields $\mathbf{E}^a$ at each site.

The appearance of two polarization terms in eq 8 is what distinguishes the present calculation of the reaction activation barrier from standard protocols[18,19,42] of electron transfer simulations based on eq 9. The calculation of cofactors polarizabilities at different levels of quantum chemistry is discussed in SI. The formalism outlined here is applied below to calculate the free-energy surfaces for two reactions listed in eq 1. The results for the reorganization energies (eqs 2 and 3) in polarizable and nonpolarizable models (eq 8 vs eq 9) are compared in Table 1. One finds $\lambda^{\mathrm{St}} < \lambda = (\lambda_1 + \lambda_2)/2$ for polarizable cofactors.

Table 1: Average values of the energy gap and reorganization energies of electron transfer (eqs 2 and 3, eV).

Reaction[a,b]	$\langle X^C\rangle_1$	$\langle X^C\rangle_2$	λ^{St}	λ_1	λ_2	$\lambda/\lambda^{\mathrm{St}}$
No polarizability corrections						
$A0^-$-F_x (dry)	−2.10	−3.81	0.85	1.29	1.16	1.44
$A0^-$-F_x (wet)	−2.10	−4.90	1.40	1.29	1.17	0.88
$A0^-$-MQ	0.96	−1.93	1.45	1.71	1.49	1.10
Polarizability included						
$A0^-$-MQ[c]	0.46	−2.30	1.38	2.36	1.68	1.46

[a]Forward reaction indicated. [b]$\lambda = (\lambda_1 + \lambda_2)/2$. [c]The reorganization energies change upon $\Delta\alpha \to 4\Delta\alpha$ rescaling to $\lambda^{\mathrm{St}} = 1.18$ eV, $\lambda_1 = 8.5$ eV, and $\lambda_2 = 5.0$ eV.

Electronic coupling. The electronic coupling V_i was calculated from 100 frames in

vacuum and in the protein environment as described in detail in SI. It was found to strongly fluctuate with changing protein configurations.[15] The standard deviation of V exceeds the mean, which thus becomes poorly defined. We therefore specify the effective coupling as the rms value

$$V_{\mathrm{eff,i}} = \sqrt{\langle V^2 \rangle_i} \tag{10}$$

where the average is taken over configurations along the simulation trajectories (Table S3).

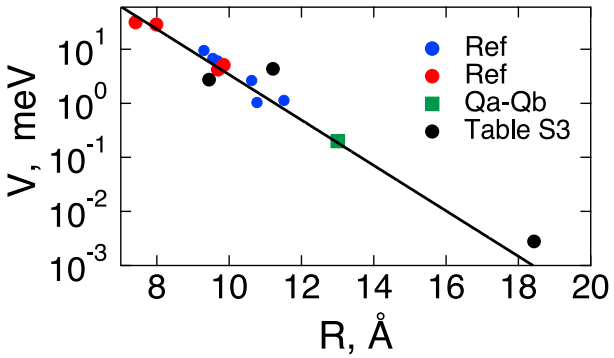

Figure 3: $V_{e,i}$ vs the center-to-center donor-acceptor distance from ref[59] compared to the Voityuk equation (solid line, eq 12).[60] The red points indicate the results from ref[55] and the green square refers to Q_A-Q_B coupling in the bacterial reaction center.[61] The black points refer to the vacuum calculations listed in Table S3.

One can assume that the main effect of protein fluctuations is through altering the donor-acceptor distance. With Gaussian fluctuations of R, one recovers the equilibrium coupling $V_{e,i}$ as

$$V_{e,i} = V_{\mathrm{eff},i} \exp\left[-\frac{1}{4}\gamma^2 \langle (\delta R)^2 \rangle_i\right] \tag{11}$$

This equation was used to compare our calculations to reported values of the electronic coupling for protein electron transfer[55,59,62] (points in Figure 3). These results were also compared to an interpolation relation provided by Voityuk[60] (solid line in Figure 3)

$$\log_{10} V_e(R) = 1.73 - 0.42(R/\text{Å}) \tag{12}$$

The parameter $\gamma = 1.934$ Å^{-1} from this equation was adopted in calculations of the dy-

namical crossover parameter discussed below. With some scatter, the calculated values of $V_{e,i}$ are consistent with the trend prescribed by eq 12 (Figure 3). Calculations of coupling between π-conjugated organic homo-dimer cations have shown that the fragment orbital density functional theory (FODFT) adopted in our calculations can underestimate coupling by $\simeq 40$ %.[63] This level of uncertainties in the electronic coupling does not strongly affect the rate calculations as we find below that the A_0-MQ reaction (eq 1) falls in the regime of dynamical control and its rate is weakly affected by the coupling magnitude (Figure 2). The coupling value affects only the distance R^* of the crossover from the dynamical control to rate's exponential decay at larger donor-acceptor separations.

A_0-F_x reaction. The trajectories for the energy gap between A_0 and F_x cofactors indicate a transition between two stationary states for the backward transition from F_x^- to A_0. These two configurations correspond to dry and wet states of F_x^-, which gains $\simeq 3$ water molecules within the radius of 3 Å after $\simeq 160$ ns of MD simulations (Figure 4a).

The free energy surfaces were calculated from energy-gap distributions in dry and wet configurations of the F_x^- site. The average value of the energy gap includes the Coulomb component $\langle X^C\rangle_i$ from MD and an unknown nonpolar energy gap $\Delta E^{\rm np}$ (eq 8)

$$\langle X\rangle_i = \Delta E^{\rm np} + \langle X^C\rangle_i \tag{13}$$

The nonpolar component $\Delta E^{\rm np}$ can thus be calculated from the experimental reaction free energy $\Delta G = -0.351$ eV (Table 2) and the mean Coulomb energy gap sampled by simulations

$$\Delta G = \Delta E^{\rm np} + X_m^C, \quad X_m^C = \frac{1}{2}\left(\langle X^C\rangle_1 + \langle X^C\rangle_2\right) \tag{14}$$

This procedure applied to the wet (equilibrium) state of the cofactor results in the free energy surfaces $F_i(X)$, $i = 1, 2$ of ET shown in Figure 4b. Assuming that $\Delta E^{\rm np}$ has the same value for the nonequilibrium water configuration, one can estimate $\Delta G^{\rm neq}$ from the above equation with X_m^C taken from the equilibrium (wet) and nonequilibrium (dry) parts of

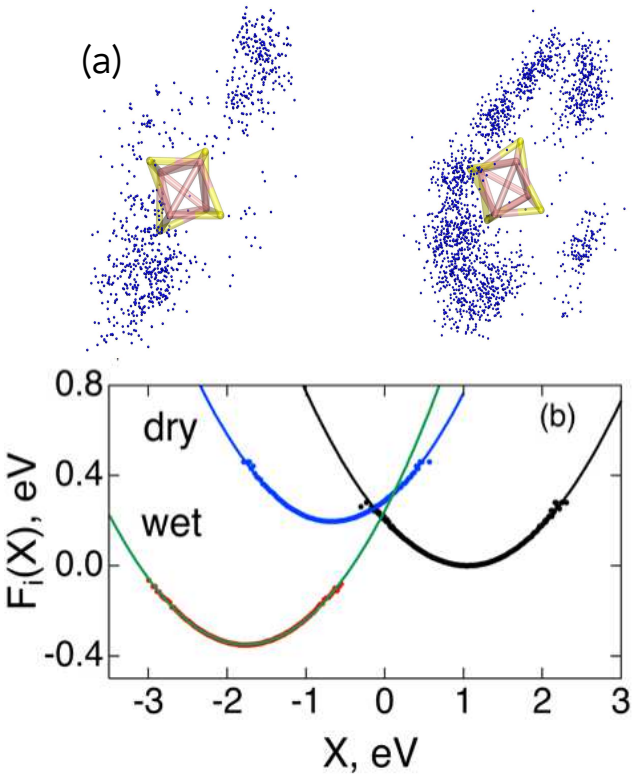

Figure 4: (a) Water molecules around the F_x cofactor taken from a 300 to 500 ns part of the trajectory. Blue dots indicate oxygen atoms of water within 5 Å form the F_x cluster atoms. Calculations are done for the forward (left) and backward (right) trajectories. (b) Free energy surfaces of electron transfer in the nonequilibrium (dry) and equilibrium (wet) water configurations. The free energy surface $F_1(X)$ (black) crosses the free energy surface $F_2(X)$ at $X = 0$ to produce the reaction Gibbs energy of -0.351 eV (Table 2), which requires $\Delta E^{\mathrm{np}} = 3.15$ eV. The points indicate results obtained from the analysis of the simulation trajectories and solid lines are fittings to shifted parabolas.

the energy gap trajectory. This procedure yields nonequilibrium free energy surface $F_2(X)$ shown in Figure 4b (labeled "wet"). The crossing point with the initial (dry) surface is slightly off the anticipated zero value, which indicates a small error of the assumption of a constant $\Delta E^{\rm np}$. The energy gap $\Delta E^{\rm np}$ includes an invariant gas-phase component and a shift due to induction interactions.[58] It is not entirely unreasonable to anticipate a small change in that latter component. Also note that the reaction becomes endergonic in the dry configuration, with the reaction Gibbs energy $\Delta G_{\rm neq} \simeq 0.25$ eV. The barrier for the forward reaction is about the same in both cases (Table 2).

Table 2: Activation barriers and non-adiabatic (NA) reaction times.

Reaction	ΔG, eV	$\Delta F^\dagger$, eV[a]	$\tau_{\rm NA}$, ns	$\tau_{\rm NA}$[b], ns
$A0^-$-F_x[c]	−0.351	0.20	1.3×10^7	5.8×10^3
$A0^-$-MQ[c,d]	−0.390	0.117	0.299	0.001
$A0^-$-MQ[e]	−0.390	0.074	0.021	0.001

[a]Correction for electronic polarization screening $f_e = 0.8$ is applied to the activation barrier. [b]At $\Delta F_1^\dagger = 0$. [c]No polarizability corrections. [d]Calculations are done with $V_{\rm eff} = 6$ meV (Table S3 and Figure 3). [e]With polarizabilities of A_0 and MQ included.

A_0-MQ reaction. A full calculation of the energy gap statistics including polarizability corrections is done for the A_0-MQ reaction. The distributions of electric field magnitudes are shown in Figure 2: the RC is characterized by strong electric fields with the average magnitude $\simeq (1-2)$ V/Å. A stronger field at the A_0 cofactor is aligned with a much higher polarizability of A_0 compared to MQ (SI). Therefore, the main effect of polarizability on the energy-gap statistics comes from the A_0 site.

The electric field alters the electron-transfer energy gap through the free energy of donor and acceptor polarization in the two last terms in eq 8. This term, quadratic in the field, makes the statistics of the energy gap non-Gaussian and leads to non-parabolic free energy surfaces of electron transfer (Figure 5b) characterized by three reorganization energies (Table 1): $\lambda^{\rm St}$ and two λ_i (eqs 2 and 3). All reorganization energies are equal within statistical uncertainties for nonpolarizable cofactors (Table 1), as expected from the canonical Marcus theory.[4] The activation barrier is the free energy difference between the crossing point at

$X = 0$ and the free-energy minimum (Figure 5 and Table 2).

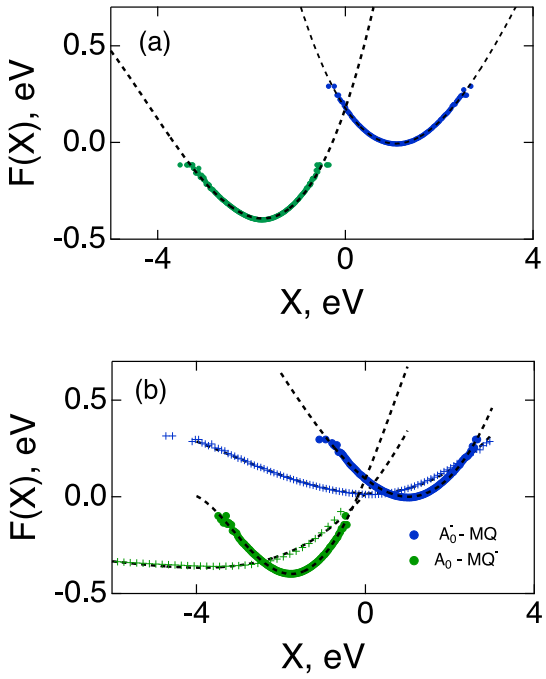

Figure 5: Free energy surfaces of A_0-MQ electron transfer (a) without and (b) with polarizability corrections for the electron-transfer cofactors. The free energy surfaces for the forward, $F_1(X)$ (blue), and backward, $F_2(X)$ (green), electron transfer are calculated from the simulation trajectories and shifted to accommodate $\Delta G = -0.390$ eV (Table 2). The points indicate results obtained from the analysis of the simulation trajectories and dashed lines are fittings to polynomials. The activation barriers to the forward reaction are 0.183 eV (a) and 0.074 eV (b) (Tables 2 and 3). Pluses in (b) indicate the results obtained by rescaling the polarizability difference $\Delta\boldsymbol{\alpha} \rightarrow 4\Delta\boldsymbol{\alpha}$ (see text for discussion).

The calculations of electric fields (Figure 2a) and of the corresponding free energy surfaces for electron transfer (Figure 5b) have been done here with the point-charge force field for all components of the thermal bath (protein, lipids, and water). A recent study of Boxer and co-workers compared electric fields produced from point-charge force fields with experimentally measured electric fields to conclude that point-charge models severely, at least by a factor of two, underestimate electric fields inside proteins.[64] This recent result agrees with previous similar estimates.[65] The theory-experiment disagreement is a deficiency of currently adopted force fields since AMOEBA force field is consistent with experiment. The average underestimate of the electric field by a factor of two projects, in our formalism, to a

polarizability change multiplied by a factor of four: $\Delta\boldsymbol{\alpha} \rightarrow 4\Delta\boldsymbol{\alpha}$. To indicate how the field correction can affect the free energy surfaces of electron transfer, Figure 5b shows the result of this rescaling. The activation barrier of the reaction disappears in this calculation. The presence of the barrier in our calculations can be another indicative of inaccuracies of present force fields since reactions between the primary acceptor and quinone cofactor are typically activationless in bacterial reaction centers.[66,67] Nevertheless, we acknowledge limitations of current schemes of polarizability calculation (Table S4)[20] putting the activation barrier in the range between the limit of $\Delta\boldsymbol{\alpha} = 0$ and no barrier obtained from polarizability rescaling.

Stokes shift and distance dynamics. The Stokes-shift dynamics are defined by the energy gap time auto-correlation function (see SI for details)

$$C_X(t) = \langle \delta X(t) \delta X(0) \rangle, \quad \delta X(t) = X(t) - \langle X \rangle. \tag{15}$$

Figure 6a shows the normalized time correlation functions $S_X(t) = C_X(t)/C_X(0)$ calculated from the trajectories of the Coulomb energy gap $X^C(t)$ (eq 9) and the total energy gap $X(t)$ (eq 9) for the forward A_0-MQ electronic transition. We find the dynamics of the energy gap $X(t)$ to be faster than of its Coulomb component $X^C(t)$ (Figure 6a). In addition, there is substantial anisotropy between the forward and backward transitions: the dynamics for the latter are much slower (Figure 6b).

Similarly to the Stokes-shift dynamics of electrostatic interactions, the dynamics of the donor-acceptor distance are anisotropic between the forward and backward transitions (Figure 6c) as indicated by the time auto-correlation function

$$C_R(t) = \langle \delta R(t) \delta R(0) \rangle, \quad \delta R(t) = R(t) - \langle R \rangle \tag{16}$$

This asymmetry can have the static origin since electronic transition results in a substantial, $\simeq 1.5$ Å, shortening of the donor-acceptor distance (Figure 6d). In addition, the variance of the donor-acceptor distance is about five times higher for A_0-MQ compared to A_0-F_x (Table

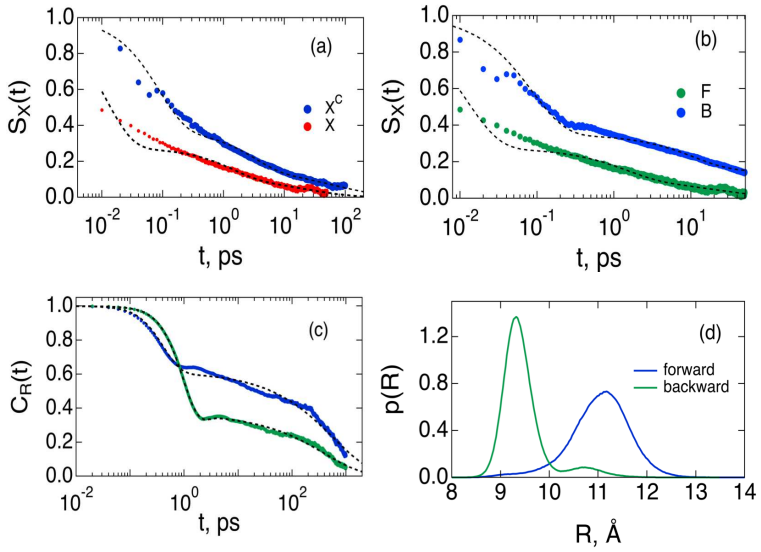

Figure 6: (a) Normalized time correlation functions $S_X(t)$ for the Coulomb component of the energy gap $X^C(t)$ (blue) and the total energy gap (eq 8) with polarizability corrections included (red) for the forward transition. (b) The normalized Stokes-shift time correlation function for the forward (green) and backward (blue) A_0-MQ transition. (c) Normalized time correlation functions of donor-acceptor distances. (d) Distributions of donor-acceptor distances for forward (blue) and backward (green) transitions. Points are correlation functions obtained from simulation trajectories and dashed lines are fits (see SI). The average relaxation times calculated from the fits are listed in Table 3.

S5) indicating loose binding of MQ compared to F_x.

Rates. The activation barrier $\Delta F^\dagger$ found from crossing of the free energy surfaces (Figure 5) is combined with the effective electronic coupling V_{eff} in the non-adiabatic rate constant calculated according to the standard golden-rule expression[14]

$$k_{\text{NA}} = A_{\text{NA}} e^{-\beta \Delta F^\dagger} \tag{17}$$

The pre-exponential factor in the rate constant is given as follows

$$A_{\text{NA}} = \frac{V_{\text{eff}}^2}{\hbar} \left(\frac{\pi \beta}{\lambda} \right)^{1/2} \tag{18}$$

The coupling for the A_0-F_x reaction is very low, $V_{\text{eff}} = 3.4 \times 10^{-6}$ eV at the average donor-acceptor center-to-center distance of 18.4 Å (Table S3). Even if the activation barrier is neglected, the activationless golden-rule reaction time $\tau_{\text{ET}} = k_{\text{NA}}^{-1}$ at this coupling magnitude becomes equal to 5.8 μs. This reaction thus cannot contribute to electron transport in HbRC by the virtue of a too low electronic coupling. The inclusion of the activation barrier of $\Delta F_1^\dagger = 0.20$ eV for the forward reaction (Figure 2) further increases the reaction time (Table 2). Superexchange electronic coupling through the Tyr residue on the electron-transfer path (Figure 1) can potentially be higher in magnitude, but cannot produce many orders of magnitude acceleration of the rate.[61,68] Our preliminary estimate of superexchange coupling puts in the range consistent with direct coupling.

Dynamical Control of Electron Transfer. The rate of electron transfer combines the nonadiabatic rate in eqs 17 and 18 with the dynamical factor $(1+g)^{-1}$ according to eq 5. The dynamical cross-over parameter g arises from the coupling of the Stokes-shift dynamics of the electron-transfer energy gap $X(t)$ with the dynamics of the donor-acceptor distance $R(t)$ modifying the electronic coupling. Accounting for both effects leads to the following equation[54]

$$g = \sqrt{2\pi} A_{\text{NA}} \tau_{\text{eff}} \tag{19}$$

Here, the nonadiabatic pre-exponential factor is according to eq 18 and the effective relaxation time is

$$\tau_{\text{eff}} = e^{\gamma^2\langle(\delta R)^2\rangle} \left\langle \frac{\tau_X}{\sqrt{2\beta\Delta F^\dagger + 4(\tau_X/\tau_R)\gamma^2\langle(\delta R)^2\rangle}} \right\rangle_\tau \tag{20}$$

In this equation, $\langle \dots \rangle_\tau$ specifies the average over the relaxation times τ_X and τ_R in multi-exponential relaxation dynamics determined by MD simulations (SI).[69] The index $i = 1, 2$ identifying the direction of electronic transition is dropped here for brevity.

A number of parameters are required for the calculation of g. The parameter γ is the inverse length of the exponential distance decay of the electronic coupling $V \propto \exp(-(\gamma/2)R)$. Given a good agreement with direct coupling calculations (Figure 3), the value $\gamma \simeq 1.93$ Å^{-1} from Voityuk's equation (eq 12) was adopted. The relaxation times for the Stokes-shift and distance dynamics, τ_X and τ_R, were taken from fits of the time correlation function (SI). Note that the effective relaxation time is enhanced by an exponential dependence on the variance of the donor-acceptor distance $\langle(\delta R)^2\rangle$ in eq 20.

The rate constants for forward and backward electron transfer have been calculated by combining the activation barriers $\Delta F^\dagger$ from crossing the free energy surfaces (Figure 5) with the dynamic correction according to eqs 5, 19, and 20. MD simulations performed here employ non-polarizable force fields and a correction for the screening of the Coulomb interactions by the electronic medium polarization is required. An empirical factor $f_e = 0.8$[22] is used here to scale the activation barrier as $f_e\Delta F^\dagger$.

Table 3: Reaction times for forward and backward electronic transitions between A_0 and MQ: $\Delta G = -0.39$ eV and $V = 6$ meV.

Reaction	$\Delta F^\dagger$, eV[a,b]	τ_X, ps	τ_R, ns	τ_{NA}, ns[c]	g	τ_{ET}, ns
A_0^--MQ	0.074	3.7	369	0.021	7.7	0.182
A_0-MQ^-	0.39	282	161	6406	68.0	334×10^3

[a]Correction for electronic polarization screening $f_e = 0.8$ is applied to the activation barrier. [b]With polarizabilities of A_0 and MQ included. [c]Calculations are done with $V_{\text{eff}} = 6$ meV (Table S3 and Figure 3).

The rate calculations (Table 3) show that electron transfer between A_0 and MQ is in the regime of dynamical control when the pre-exponential factor of the reaction rate constant is

specified by coupled dynamics of the energy gap and the donor-acceptor distance. A large value of the crossover parameter slows the reaction down compared to the golden rule (nonadiabatic) prediction. The reaction times is thus $\simeq$ 182 ps for the forward transition. The value of the crossover parameter g is much greater for the backward transition, contributing to a large asymmetry between the forward and backward rates.

Discussion

This study of protein electron transfer aims at two goals: (i) to clarify the mechanism of electron transfer in HbRC and (ii) to address a more general question of what might potentially be special about proteins, and specifically reaction centers, allowing fast vectorial electron transport. In particular, the issue of a specific direction of electron flow is relevant to conditions of low driving forces typically found in natural charge-transfer systems.[6] According to thermodynamics, such reactions should be fully reversible and no specific directionality of charge transport can be allowed. A related question is how proteins accomplish low activation barriers required for biological electron transport[70] and high conductivity of proteins.[32] From a more technical perspective of protein electron transfer studied by computer simulations,[19] one has to address the disconnect between high activation barriers typically found in force-field simulations and much lower barriers extracted from kinetic data.[25–29] A number of general mechanistic features have been identified in this study of HbRC, which can potentially be extended to other reaction centers of natural photosynthesis and protein complexes of respiration chains.

We have argued[71] that high intensity inhomogeneous electric fields typically measured inside proteins[3] can combine with conjugate (and polarizable) cofactors of bacterial photosynthesis to lower activation barriers for electronic transitions. We indeed find here that the most polarizable cofactor A_0 is strategically positioned at the protein site with an intense electric field much higher than the field at the less polarizable MQ cofactor. This new

physics leads to highly non-parabolic free-energy surfaces of electron transfer (Figure 5). The activation barrier for the forward transition between A_0 and MQ is strongly reduced due to polarizability effects. The presence of strong inhomogeneous electric fields at cofactors of electron-transfer chains can potentially be viewed as a design principle contributing to lowering of otherwise high activation barriers.

Our calculations of the electronic coupling involved in two electron-transfer reactions between A_0 and two acceptors, MQ and F_x, are consistent with the results presented in the literature and follow a generic exponential falloff with the donor-acceptor distance (Figure 3). A large distance between A_0 and F_x (Figure 1) effectively eliminates this reaction channel from the reaction mechanism. In contrast, electron transfer between A_0 and MQ occurs on the reaction time of $\sim$ 200 ps, consistent with the reaction time of $\sim$ 200 ps between the primary acceptor and the quinone cofactor in bacterial reaction centers.[31,67] The rate constant falls close to the end of the rate constant plateau as a function of the donor-acceptor distance (Figure 2). This observation might imply that the distance between A_0 and MQ in the reaction center is the largest separation permitting a sufficiently fast reaction, before slowing down with increasing separation due to less probable tunneling.

The appearance of a plateau in the distance dependence of the reaction rate (Figure 2) is the consequence of dynamical control of electron transfer, when friction outcompetes the rate of tunneling in the reaction activated state.[57] The dynamical crossover parameter governs the turnover at the effective distance R^* specified by the condition $g(R^*) = 1$ (eq 5). The value of $g(R)$ is affected by electronic coupling and coupled dynamics[54] of electrostatic interactions (Stokes-shift dynamics) and of the donor-acceptor distance (Figure 6).

A surprising finding of this study is a substantial dynamical anisotropy between the forward and backward electronic transitions: the Stokes-shift dynamics are much slower for the backward transition. Correspondingly, the dynamical crossover parameter g is much higher for the backward reaction (Table 3). This dynamical anisotropy promotes vectorial charge transfer, which is achieved by a combination of thermodynamic (driving force) and dynam-

ical factors. The detailed balance between forward and backward reaction rates requires an effective reaction free energy ΔG_{eff}

$$\Delta G_{\text{eff}} = \Delta G_0 - k_{\text{B}} T \ln [g_2/g_1] \tag{21}$$

This relation predicts about $\simeq -59$ mV additional reaction Gibbs energy originating from an order of magnitude difference between the backward and forward crossover parameters (Table 3).

One can speculate about specific mechanisms behind such dynamical anisotropy in protein media. Proteins are closely packed systems similar to low-temperature liquids (packing fraction $\simeq 0.6$[72]). The dynamics in such media can be strongly affected by relatively small structural changes.[73] Our simulations show that the arrival of the electron to a redox cofactor can produce structural changes altering the medium relaxation times by potentially orders of magnitude. The corresponding effect on the reaction rate constant, through the factor g^{-1} in the reaction rate pre-exponential factor, makes the backward reaction much slower than anticipated from solely thermodynamic arguments.

The mechanism of charge transport in HbRC is not fully established at this moment.[37] Consistent with charge transport in other bacterial reaction centers,[31,67] we predict the transition from the primary acceptor (A_0) to the menaquinone (MQ) cofactor with the reaction time of ~ 200 ps. The backward reaction is predicted to have the reaction time of $\simeq 0.3$ ms (Table 3). The next step in the electron transport chain, currently unknown, should thus happen within a sub-ms reaction time to compete with the backward MQ-A_0 transition.

Supporting Information Available

Simulation protocol, derivation of equations, and the analysis of time correlation functions from MD simulations.

Notes

The authors declare no competing financial interests.

Acknowledgement

This material is based upon work supported by the U.S. Department of Energy, Office of Science, Office of Basic Energy Sciences Energy Frontier Research Centers program under Award Number DE-SC-0010575 and by the National Science Foundation (CHE-2154465). The supercomputer time was provided through Extreme Science and Engineering Discovery Environment (XSEDE) allocation MCB080071 and through ASU's Research Computing. We are grateful to Kevin Redding for insightful discussions.

References

(1) Pauling, L. Molecular architecture and biological reactions. *Chem. Eng. News* **1946**, *24*, 1375–1377.

(2) Fried, S. D.; Bagchi, S.; Boxer, S. G. Extreme electric fields power catalysis in the active site of ketosteroid isomerase. *Science* **2014**, *346*, 1510–1514.

(3) Fried, S. D.; Boxer, S. G. Electric fields and enzyme catalysis. *Ann. Rev. Biochem.* **2017**, *86*, 387–415.

(4) Marcus, R. A.; Sutin, N. Electron transfer in chemistry and biology. *Biochim. Biophys. Acta* **1985**, *811*, 265–322.

(5) Warshel, A. Dynamics of reactions in polar solvents. Semiclassical trajectory studies of electron-transfer and proton-transfer reactions. *J. Phys. Chem.* **1982**, *86*, 2218–2224.

(6) Nicholls, D. G.; Ferguson, S. J. *Bioenergetics4*; Academic Press: Amsterdam, 2013.

(7) Warshel, A.; Sharma, P. K.; Kato, M.; Xiang, Y.; Liu, H.; Olsson, M. H. M. Electrostatic basis for enzyme catalysis. *Chem. Rev.* **2006**, *106*, 3210–3235.

(8) Matyushov, D. V. Protein electron transfer: is biology (thermo)dynamic? *J. Phys.: Condens. Matter* **2015**, *27*, 473001.

(9) Henzler-Wildman, K.; Kern, D. Dynamic personalities of proteins. *Nature* **2007**, *450*, 964–972.

(10) Cheatum, C. M. Low-frequency protein motions coupled to catalytic sites. *Ann. Rev. Phys. Chem.* **2020**, *71*, 267–288.

(11) Schafer, J. W.; Schwartz, S. D. Directed evolution's influence on rapid density fluctuations illustrates how protein dynamics can become coupled to chemistry. *ACS Catalysis* **2020**, *10*, 8476–8484.

(12) Gray, H. B.; Winkler, J. R. Electron tunneling through proteins. *Quart. Rev. Biophys.* **2003**, *36*, 341–372.

(13) Gray, H. B.; Winkler, J. R. Long-range electron transfer. *Proc. Natl. Acad. Sci.* **2005**, *102*, 3534–3539.

(14) Levich, V. G. In *Advances in Electrochemistry and Electrochemical Engineering*; Delahay, P., Ed.; Interscience: New York, 1965; Vol. 4; pp 1–124.

(15) Skourtis, S. S.; Waldeck, D. H.; Beratan, D. N. Fluctuations in biological and bioinspired electron-transfer reactions. *Annu. Rev. Phys. Chem.* **2010**, *61*, 461–485.

(16) Migliore, A.; Polizzi, N. F.; Therien, M. J.; Beratan, D. N. Biochemistry and theory of proton-coupled electron transfer. *Chem. Rev.* **2014**, *114*, 3381–3465.

(17) Moser, C. C.; Page, C. C.; Cogdell, R. J.; Barber, J.; Wraight, C. A.; Dutton, P. L. *Adv. in Protein Chem.*; Elsevier, 2003; Vol. 63; p 71.

(18) Matyushov, D. V. Protein electron transfer: Dynamics and statistics. *J. Chem. Phys.* **2013**, *139*, 025102.

(19) Blumberger, J. Recent advances in the theory and molecular simulation of biological electron transfer reactions. *Chem. Rev.* **2015**, *115*, 11191–11238.

(20) Sarhangi, S. M.; Matyushov, D. V. Comment on "Applicability of perturbed matrix method for charge transfer studies at bio/metallic interfaces: a case of azurin" by O. Kontkanen, D. Biriukov and Z. Futera, Phys. Chem. Chem. Phys. , 2023, 25 , 12479. *Phys. Chem. Chem. Phys.* **2023**, *25*, 26923–26928.

(21) Warshel, A.; Parson, W. W. Computer simulations of electron-transfer reactions in solution and in photosynthetic reaction centers. *Annu. Rev. Phys. Chem.* **1991**, *42*, 279–309.

(22) Matyushov, D. V. Reorganization energy of electron transfer. *Phys. Chem. Chem. Phys.* **2023**, *25*, 7589–7610.

(23) Jiang, X.; Futera, Z.; Blumberger, J. Ergodicity-breaking in thermal biological electron transfer? Cytochrome *c* revisited. *J. Phys. Chem. B* **2019**, *123*, 7588–7598.

(24) Gupta, S.; Matyushov, D. V. Effects of solvent and solute polarizability on the reorganization energy of electron transfer. *J. Phys. Chem. A* **2004**, *108*, 2087–2096.

(25) Guo, Y.; Zhao, J.; Yin, X.; Gao, X.; Tian, Y. Electrochemistry investigation of protein protection by alkenthiol self-assembled monolayers against urea impact. *J. Phys. Chem. C* **2008**, *112*, 6013–6021.

(26) Khoshtariya, D. E.; Dolidze, T. D.; Shushanyan, M.; Davis, K. L.; Waldeck, D. H.; van Eldik, R. Fundamental signatures of short- and long-range electron transfer for the blue copper protein azurin at Au/SAM junctions. *Proc. Natl. Acad. Sci. USA* **2010**, *107*, 2757–2762.

(27) Zitare, U. A.; Szuster, J.; Santalla, M. C.; Morgada, M. N.; Vila, A. J.; Murgida, D. H. Dynamical effects in metalloprotein heterogeneous electron transfer. *Electrochim. Acta* **2020**, *342*, 136095.

(28) Alessandrini, A.; Corni, S.; Facci, P. Unravelling single metalloprotein electron transfer by scanning probe techniques. *Phys. Chem. Chem. Phys.* **2006**, *8*, 4383–4397.

(29) Zheng, Z.; Grall, S.; Kim, S. H.; Chovin, A.; Clement, N.; Demaille, C. Activationless electron transfer of redox-DNA in electrochemical nanogaps. *J. Am. Chem. Soc.* **2024**, *146*, 6094–6103.

(30) Blankenship, R. E. *Molecular Mechanisms of Photosynthesis*; Blackwell Science: Williston, VT, 2003.

(31) Hoff, A. J.; Deisenhofer, J. Photophysics of photosynthesis. *Phys. Rep.* **1997**, *287*, 1–247.

(32) Amdursky, N.; Marchak, D.; Sepunaru, L.; Pecht, I.; Sheves, M.; Cahen, D. Electronic transport via proteins. *Adv. Mat.* **2014**, *26*, 7142–7161.

(33) Zhang, B.; Song, W.; Pang, P.; Lai, H.; Chen, Q.; Zhang, P.; Lindsay, S. Role of contacts in long-range protein conductance. *Proc. Natl. Acad. Sci. USA* **2019**, *116*, 5886–5891.

(34) Lindsay, S. Ubiquitous electron transport in non-electron transfer proteins. *Life* **2020**, *10*, 72–13.

(35) Gu, Y.; Srikanth, V.; Salazar-Morales, A. I.; Jain, R.; O'Brien, J. P.; Yi, S. M.; Soni, R. K.; Samatey, F. A.; Yalcin, S. E.; Malvankar, N. S. Structure of Geobacter pili reveals secretory rather than nanowire behaviour. *Nature* **2021**, *597*, 430–434.

(36) Shipps, C.; Kelly, H. R.; Dahl, P. J.; Yi, S. M.; Vu, D.; Boyer, D.; Glynn, C.; Sawaya, M. R.; Eisenberg, D.; Batista, V. S. et al. Intrinsic electronic conductivity

of individual atomically resolved amyloid crystals reveals micrometer-long hole hopping via tyrosines. *Proc. Natl. Acad. Sci. USA* **2021**, *118*, e2014139118.

(37) Gisriel, C.; Sarrou, I.; Ferlez, B.; Golbeck, J. H.; Redding, K. E.; Fromme, R. Structure of a symmetric photosynthetic reaction center–photosystem. *Science* **2017**, *357*, 1021–1025.

(38) Gupta, R. S. Evolutionary relationships among photosynthetic bacteria. *Photosynthesis research* **2003**, *76*, 173–183.

(39) Olsen, J. M. H.; Kongsted, J. In *Adv. Quant. Chem.*; Sabin, J. R., Brändas, E., Eds.; Academic Press, 2011; Vol. 61; pp 107–143.

(40) Frederiksen, A.; Gerhards, L.; Reinholdt, P.; Kongsted, J.; Solov'yov, I. A. Importance of polarizable embedding for absorption spectrum calculations of arabidopsis thaliana cryptochrome 1. *J. Phys. Chem. B* **2024**, *128*, 6283–6290.

(41) Di Prima, D.; Reinholdt, P.; Kongsted, J. Color tuning in bovine rhodopsin through polarizable embedding. *J. Phys. Chem. B* **2024**, *128*, 2864–2873.

(42) Small, D. W.; Matyushov, D. V.; Voth, G. A. The theory of electron transfer: What may be missing? *J. Am. Chem. Soc.* **2003**, *125*, 7470–7478.

(43) Dinpajooh, M.; Martin, D. R.; Matyushov, D. V. Polarizability of the active site of cytochrome *c* reduces the activation barrier for electron transfer. *Sci. Rep.* **2016**, *6*, 28152.

(44) Martin, D. R.; Dinpajooh, M.; Matyushov, D. V. Polarizability of the active site in enzymatic catalysis: Cytochrome c. *J. Phys. Chem. B* **2019**, *123*, 10691–1069.

(45) Boxer, S. G. Stark Realities. *J. Phys. Chem. B* **2009**, *113*, 2972–2983.

(46) Matyushov, D. V.; Voth, G. A. Modeling the free energy surfaces of electron transfer in condensed phases. *J. Chem. Phys.* **2000**, *113*, 5413–5424.

(47) Moser, C. C.; Keske, J. M.; Warncke, K.; Farid, R. S.; Dutton, P. L. Nature of biological electron transfer. *Nature* **1992**, *355*, 796–802.

(48) Gray, H. B.; Winkler, J. R. Functional and protective hole hopping in metalloenzymes. *Chem. Sci.* **2021**, *12*, 13988–14003.

(49) Zusman, L. D. Outer-sphere electron transfer in polar solvents. *Chem. Phys.* **1980**, *49*, 295–304.

(50) Sumi, H.; Marcus, R. A. Dynamical effects in electron transfer reactions. *J. Chem. Phys* **1986**, *84*, 4894–4914.

(51) Hynes, J. T. Outer-sphere electron-transfer reactions and frequency-dependent friction. *J. Phys. Chem.* **1986**, *90*, 3701–3706.

(52) Rips, I.; Jortner, J. Dynamic solvent effects on outer-sphere electron transfer. *J. Chem. Phys.* **1987**, *87*, 2090–2104.

(53) Maroncelli, M.; Fleming, G. R. Picosecond solvation dynamics of coumarin-153: The importance of molecular aspects of solvation. **1987**, *86*, 6221.

(54) Matyushov, D. V. Conformational dynamics modulating electron transfer. *J. Chem. Phys.* **2022**, *157*, 095102.

(55) Sarhangi, S. M.; Matyushov, D. V. Electron tunneling in biology: When does it matter? *ACS Omega* **2023**, *8*, 27355–27365.

(56) Kramers, H. Brownian motion in a field of force and the diffusion model of chemical reactions. *Physica* **1940**, *7*, 284–304.

(57) Frauenfelder, H.; Sligar, S. G.; Wolynes, P. G. The energy landscapes and motions of proteins. *Science* **1991**, *254*, 1598–1603.

(58) LeBard, D. N.; Matyushov, D. V. Protein-water electrostatics and principles of bioenergetics. *Phys. Chem. Chem. Phys.* **2010**, *12*, 15335–15348.

(59) Guberman-Pfeffer, M. J. Assessing thermal response of redox conduction for anti-Arrhenius kinetics in a microbial cytochrome nanowire. *J. Phys. Chem. B* **2022**, *126*, 10083–10097.

(60) Voityuk, A. A. Electron transfer between [4Fe–4S] clusters. *Chem. Phys. Lett.* **2010**, *495*, 131–134.

(61) Tamura, H.; Saito, K.; Ishikita, H. Long-range electron tunneling from the primary to secondary quinones in photosystem II enhanced by hydrogen bonds with a nonheme Fe complex. *J. Phys. Chem. B* **2021**, *125*, 13460–13466.

(62) Sugo, Y.; Tamura, H.; Ishikita, H. Electron transfer route between quinones in type-II reaction centers. *J. Phys. Chem. B* **2022**, *126*, 9549–9558.

(63) Kubas, A.; Hoffmann, F.; Heck, A.; Oberhofer, H.; Elstner, M.; Blumberger, J. Electronic couplings for molecular charge transfer: Benchmarking CDFT, FODFT, and FODFTB against high-level ab initio calculations. *J. Chem. Phys.* **2014**, *140*, 104105.

(64) Kirsh, J. M.; Weaver, J. B.; Boxer, S. G.; Kozuch, J. Critical evaluation of polarizable and nonpolarizable force fields for proteins using experimentally derived nitrile electric fields. *J. Am. Chem. Soc.* **2024**, *146*, 6983–6991.

(65) Vaissier, V.; Sharma, S. C.; Schaettle, K.; Zhang, T.; Head-Gordon, T. Computational optimization of electric fields for improving catalysis of a designed kemp eliminase. *ACS Catalysis* **2018**, *8*, 219–227.

(66) Laporte, L.; Kirmaier, C.; Schenck, C. C.; Holten, D. Free-energy dependence of the rate of electron transfer to the primary quinone in beta-type reaction centers. *Chem. Phys.* **1995**, *97*, 225–237.

(67) LeBard, D. N.; Martin, D. R.; Lin, S.; Woodbury, N. W.; Matyushov, D. V. Protein dynamics to optimize and control bacterial photosynthesis. *Chem. Sci.* **2013**, *4*, 4127–4136.

(68) Saito, K.; Tamura, H.; Ishikita, H. Superexchange electron transfer and protein matrix in the charge-separation process of photosynthetic reaction centers. *J. Phys. Chem. Lett.* **2024**, *15*, 9183–9192.

(69) Matyushov, D. V. Nonergodic complex medium dynamics affecting protein electron transfer. *J. Chem. Phys.* **2024**, 0.26434/chemrxiv–2024–6mnwj.

(70) Dahl, P. J.; Yi, S. M.; Gu, Y.; Acharya, A.; Shipps, C.; Neu, J.; O'Brien, J. P.; Morzan, U. N.; Chaudhuri, S.; Guberman-Pfeffer, M. J. et al. A 300-fold conductivity increase in microbial cytochrome nanowires due to temperature-induced restructuring of hydrogen bonding networks. *Sci. Adv.* **2022**, *8*, eabm7193.

(71) LeBard, D. N.; Kapko, V.; Matyushov, D. V. Energetics and kinetics of primary charge separation in bacterial photosynthesis. *J. Phys. Chem. B* **2008**, *112*, 10322–10342.

(72) Gaines, J. C.; Clark, A. H.; Regan, L.; O'Hern, C. S. Packing in protein cores. *J. Phys.: Condens. Matter* **2017**, *29*, 293001–16.

(73) Angell, C. A. Formation of glasses from liquids and biopolymers. *Science* **1995**, *267*, 1924–1935.